

Regularizing made-to-measure particle models of galaxies

Lucia Morganti^{1*} and Ortwin Gerhard^{1†}

¹ *Max-Planck-Institut für extraterrestrische Physik, Postfach 1312, Giessenbachstr., D-85741 Garching, Germany*

Accepted 2012 February 9. Received 2012 February 9; in original form 2011 December 20.

ABSTRACT

Made-to-measure methods such as the parallel code NMAGIC are powerful tools to build galaxy models reproducing observational data. They work by adapting the particle weights in an N-body system until the target observables are well matched. Here we introduce a moving prior regularization (MPR) method for such particle models. It is based on determining from the particles a distribution of priors in phase-space, which are updated in parallel with the weight adaptation. This method allows one to construct smooth models from noisy data without erasing global phase-space gradients. We first apply MPR to a spherical system for which the distribution function can in theory be uniquely recovered from idealized data. We show that NMAGIC with MPR indeed converges to the true solution with very good accuracy, independent of the initial particle model. Compared to the standard weight entropy regularization, biases in the anisotropy structure are removed and local fluctuations in the intrinsic distribution function are reduced. We then investigate how the uncertainties in the inferred dynamical structure increase with less complete and noisier kinematic data, and how the dependence on the initial particle model also increases. Finally, we apply the MPR technique to the two intermediate-luminosity elliptical galaxies NGC 4697 and NGC 3379, obtaining smoother dynamical models in luminous and dark matter potentials.

Key words: galaxies: kinematics and dynamics – methods: numerical – methods: N-body simulations

1 INTRODUCTION

In galactic dynamics, the modelling of photometric and kinematic observations is of great importance to infer intrinsic properties of galaxies such as their orbital structure, total gravitational potential, and phase-space distribution function (DF). As tautly summarized by Syer & Tremaine (1996, hereafter ST96), different techniques to create made-to-measure systems reproducing the observational data have been devised, and can be broadly grouped in DF-based, moment-based, orbit-based, and particle-based methods.

DF-based methods fit observations with parametrized functions of the integrals of motion or of the action integrals of orbits. Applications include spherical or integrable systems (*e.g.* Dejonghe 1986; Dejonghe & de Zeeuw 1988; Gerhard 1991; Hunter & de Zeeuw 1992; Carollo et al. 1995; Kronawitter et al. 2000), axisymmetric models (*e.g.* Hunter & Qian 1993; Dehnen & Gerhard 1994; Kuijken 1995; Magorrian 1995; Merritt 1996), and nearly integrable potentials (*e.g.* Dehnen & Gerhard 1993;

Matthias & Gerhard 1999; Binney 2010). The main advantage of these methods is that they provide the phase-space DF directly, although they generally require assumptions on the symmetry of the target galaxy.

Moment-based methods find solutions of the Jeans equations that best reproduce observed quantities such as surface density and velocity dispersion (*e.g.* Young 1980; Binney & Mamon 1982; Binney et al. 1990; Magorrian & Binney 1994; Lokas 2002; Cappellari 2008; Williams et al. 2009; Cappellari et al. 2009). Among the drawbacks of these methods are the need for assumptions to close the system of equations, the lack of any guarantee on the positivity of the underlying DF, and the difficulties in modelling higher order information such as the line-of-sight velocity distribution (LOSVD).

Orbit-based methods (Schwarzschild 1979, 1993) compute a large library of orbits in a fixed potential, and then adjust the weight of each orbit until the photometry and kinematics of the target galaxy are well matched (*e.g.* Richstone & Tremaine 1985; Rix et al. 1997; van der Marel et al. 1998; Cretton et al. 1999; Cappellari et al. 2002, 2006; Gebhardt et al. 2003; Valluri et al. 2004; Thomas et al. 2005, 2009;

* E-mail: morganti@mpe.mpg.de

† E-mail: gerhard@mpe.mpg.de

van den Bosch & de Zeeuw 2010). Schwarzschild modelling is widely used, *e.g.* to infer the masses of black holes at the centers of galaxies, but applications are mostly restricted to axisymmetric systems. Moreover, the technique requires the computation of a large and representative orbit library for every new trial potential.

Particle-based methods for the most part work by slowly correcting individual weights of particles as they are evolved in the gravitational potential (ST96), until the N -body system reproduces the observational data. Kinematic and density observables can be used simultaneously in the weight correction by minimizing χ^2 -deviations between data and particle model (de Lorenzi et al. 2007, hereafter DL07). Among the main strengths of this so-called made-to-measure (M2M) technique are its geometric flexibility, the fact that the potential can be evolved self-consistently from the particles, and that there is no need to store an orbit library.

The M2M method was first applied to the Milky Way's bulge and disk in Bissantz et al. (2004). A version modified to model observational data with errors (χ^2 M2M) was implemented in the parallel code NMAGIC by DL07. This has been used to investigate the dynamics of the outer halos of the two intermediate-luminosity elliptical galaxies NGC 4697 and NGC 3379 (de Lorenzi et al. 2008, 2009, hereafter DL08; DL09), and of the massive elliptical galaxy NGC 4649 (Das et al. 2011). More recent implementations of the M2M method can be found in Dehnen (2009), who proposed a different technique for the weight adaptation, and Long & Mao (2010). A related particle method but with a different way of adjusting to the observational constraints is the iterative technique of Rodionov et al. (2009).

M2M techniques are very promising, but relatively unexplored. It is therefore a natural question whether these particle methods can actually recover the phase-space DF of a target galaxy if the data uniquely specify it. For a given set of data, how much does the final particle model depend on the initial one? And how is this dependence influenced by incomplete or noisy data? Furthermore, given that a system of N particles is trained to match a much smaller number of observational constraints, the problem arises of reducing model degeneracies and preventing the method from fitting the noise in the data.

The above issues are related and are connected to the concept of regularization. In standard χ^2 M2M practice, a weight entropy is used to regularize the particle model: through the entropy function all particle weights are biased towards a smooth distribution of predefined priors, which are specified together with the initial model, and thus implicitly contain assumptions about the dynamical structure of the target galaxy. Therefore, unless the dynamical structure of the galaxy is known beforehand, smoothing with weight entropy makes it difficult to construct models with strong phase-space gradients, *e.g.* between near-radial and near-circular orbits. This is discussed further in Section 2. A similar effect arises in Schwarzschild models regularized using maximum-entropy constraints (Richstone & Tremaine 1988), which tend to isotropize the final DF (*e.g.* Thomas et al. 2005).

In this paper, we describe a new Moving Prior entropy Regularization (MPR) method based on the idea of a distribution of particle priors, which are computed according to phase-space occupation and which evolve together with the

adaptation of the particle weights. The new method minimizes the dependence of the solution on the adopted initial particle model, and facilitates recovering both a smoother and more accurate DF, reducing local fluctuations without erasing global phase-space gradients.

The paper is organized as follows. In Section 2 the basics of the χ^2 M2M method are laid out, the main concerns related to the traditional regularization are explained, and our implementation of MPR is developed. In Section 3 a series of spherical target models is constructed for testing the M2M method with MPR. Then, in Section 4 and 5 we investigate the different roles played by regularization, initial particle model, and data quality for recovering the correct galaxy model, and we show that the true solution can indeed be recovered from sufficiently good data. Finally, two astrophysical applications are presented in Section 6, where we reconstruct regularized NMAGIC models for the elliptical galaxies NGC 4697 and NGC 3379 in their dark matter halos. The paper closes in Section 7.

2 REGULARIZATION OF PARTICLE MODELS

In this Section we outline the χ^2 M2M method, and discuss some issues related to its standard (weight entropy) regularization. An alternative method to regularize M2M particle models is then presented. For a more detailed description of the M2M technique we refer the reader to ST96, DL07, Dehnen (2009), and Long & Mao (2010).

2.1 Brief review of χ^2 M2M technique to model observational data

The goal of the χ^2 M2M method is to evolve an N -body system of particles orbiting in a potential to make it reproduce the observables of a target galaxy. The potential can be either fixed and known *a priori*, or time-varying and self-consistently computed from the particles.

Each particle is characterized by its phase-space coordinates $\mathbf{z}_i = (\mathbf{r}_i, \mathbf{v}_i)$ and by a weight w_i . The particles should be interpreted in a probabilistic sense: they do not represent single stars but rather phase-space fluid elements (*e.g.* Hernquist & Ostriker 1992). If M is the total stellar mass of the system, then individual particles have masses $m_i = w_i M / \sum_{i=1}^N w_i$.

An observable of a target galaxy characterized by a distribution function $f(\mathbf{z})$ is defined as

$$Y_j = \int K_j(\mathbf{z}) f(\mathbf{z}) d^6z, \quad (1)$$

where K_j is an appropriate kernel and $\mathbf{z} = (\mathbf{r}, \mathbf{v})$ are the phase-space coordinates.

Given a set of observables Y_j , $j = 1, \dots, J$, including *e.g.* photometry and kinematics, the particle weights w_i of the N -body system are evolved until the model observables

$$y_j(t) = \sum_{i=1}^N w_i K_j[\mathbf{z}_i(t)] \quad (2)$$

agree with the target observables Y_j . Here, the kernel includes a selection function which ensures that only particles with a direct effect on the observable y_j contribute to it.

Commonly, the model observables are replaced by their time-averaged values

$$\tilde{y}_j(t) = \alpha \int_0^\infty y_j(t - \tau) e^{-\alpha\tau} d\tau \quad (3)$$

to increase the effective number of particles contributing to them, and to reduce temporal fluctuations.

The task of adapting individual weights of orbiting particles until the target and the model observables match is accomplished by solving the set of differential equations referred to as “force-of-change”:

$$\frac{dw_i(t)}{dt} = \varepsilon w_i(t) \left(\mu \frac{\partial S}{\partial w_i} - \sum_j \frac{K_j [z_i(t)]}{\sigma(Y_j)} \Delta_j(t) \right), \quad (4)$$

where ε is a small positive constant, and the meaning of the other variables is clarified below.

Equation (4) maximizes the merit function

$$F = -\frac{1}{2}\chi^2 + \mu S \quad (5)$$

with respect to the particle weights w_i . Here

$$\chi^2 = \sum_{j=1}^J \Delta_j^2 \quad (6)$$

is a statistical measurement of the goodness of the fit in terms of deviations

$$\Delta_j(t) = \frac{\tilde{y}_j - Y_j}{\sigma(Y_j)} \quad (7)$$

between target and model observables, taking the error $\sigma(Y_j)$ of the target observable into account.

For the regularization functional, the weight entropy

$$S = -\sum_{i=1}^N w_i \log(w_i/\hat{w}_i) \quad (8)$$

is a common choice. S is a measure of the plausibility of the model in terms of the smoothness of the weight distribution and thus, indirectly, of the resulting DF, and it serves the purpose of regularization by pushing the particle weights towards some smooth predetermined weights \hat{w}_i , called priors. In typical applications the number of particles is much higher than the number of data constraints on the particle model; this intrinsic ill-conditioning of the problem translates into a large freedom in the weight adaptation, and results in models fitting the noise in the data. That is why a simple minimization of χ^2 is not a well-defined procedure to determine the model uniquely, and a certain degree of regularization is necessary.

The balance between regularization and fit to observational constraints in equation (5) is controlled by the constant μ , so that generally models with smaller μ aim for better fits to the data, but models with larger μ have smoother DFs. In practice, the best choice of μ is case dependent (see *e.g.* Gerhard et al. 1998; Thomas et al. 2005, DL08, DL09), hinging on the specific properties of the observational data to be modelled (error bars, scatter, spatial coverage), the phase-space structure of the galaxy, and possibly also the adopted initial particle model.

Finally, note that a likelihood term can be added to equation (5) to account for the constraints from a sample of discrete velocities, as derived in DL08.

2.2 Issues with standard weight entropy regularization

In the framework of the χ^2 M2M method summarized above, individual particle weights are slowly adjusted according to a compromise between χ^2 , which pushes them to match the target observables, and entropy S , which instead penalises against deviations of the weights from the preassigned set $\{\hat{w}_i\}$ of priors; more precisely, from $\{\hat{w}_i/e\}$ (see equations [5] and [8]).

Even though no rule on the choice of the priors exists, they are traditionally set to $\hat{w}_i = w_0 = 1/N$ (the “uninformative” or “flat” priors in Bayesian statistics), and the same is done for the individual weights of the initial particle model. Through the weight adaptation (4), then, the standard Global Weight entropy Regularization (hereafter GWR) encourages a dynamical structure in the particle model which is similar to that of the initial particle system. Of course, this bias is stronger for larger values of μ , and wherever the constraining power of the data is smaller, *e.g.* in the outer galactic regions.

In practice, smoothing the weights globally towards a set of preassigned, flat priors through the entropy (8) makes it difficult to reproduce strong phase-space gradients of the target galaxy, *e.g.* strongly anisotropic velocity distributions, unless either the right orbital structure is already in place in the initial particle model, *i.e.* its dynamics is known beforehand, or a very small value of μ is adopted at the expense of smoothness of the underlying DF. This was noticed both in DL08 (see their Fig. 10) and DL09, where under-smoothed models proved necessary to recover strong radial anisotropy in their elliptical galaxy models.

However, under-smoothed particle models do not represent a proper solution. Indeed, sufficient regularization is needed not only to prevent the model from fitting the noise in the data, but also to oppose fluctuations of the particle weights caused by the noise in the data, and to ensure that the weight distribution on neighbouring phase-space tori remains continuous, as intuitively expected for a relaxed stellar system.

In what follows we present a new regularization method which alleviates the main issues of the standard global weight entropy smoothing, and permits smooth M2M particle models to be obtained that reproduce the phase-space gradients of the target galaxies independently of initial conditions.

2.3 Alternative regularization based on moving priors

The logical step forward to ease the issues with the GWR is to abandon the idea of constant priors defined along with the initial particle distribution. Instead we will determine a smooth distribution of particle priors which follows the phase-space structures traced by the weight distribution, as the weight distribution evolves to match the observational data. Then we will use the weight entropy to bias particle weights towards such moving priors.

This procedure, which we will denote as Moving Prior entropy Regularization (MPR) should facilitate a smooth DF without erasing larger-scale phase-space gradients. In terms of orbits, this means that the new regularization

should assign the same prior to particles belonging to the same orbit, similar priors to particles on nearby orbits, and different priors to particles moving on very different orbits, as required in the presence of strong velocity anisotropy.

2.3.1 Assignment of new local priors

Therefore, based on Jeans' theorem (*e.g.* Binney & Tremaine 2008), the assignment of new individual priors which mirror the underlying evolving DF is best based on the integrals of motion, respectively orbits, of the particles. This is particularly simple in the spherical case, where the integrals of motion are known and can be easily found from the particle model. As already pointed out by DL09, the need for regularization is also strongest for spherical models, due to their larger number of independent orbits with respect to less symmetric systems. The aim of the present paper is to show that this method works, and how well it works, in the spherical case. A simple axisymmetric scheme is shown in Section 6, and generalizations to more complicated geometries are sketched out in Section 7.

For assigning priors in the spherical case, in practice we sort the particles according to their energy E and total angular momentum into a rectangular (E, x) grid, where the so called circularity integral $x = L/L_c$ is the ratio between the actual angular momentum and the angular momentum L_c which a circular orbit would have at the given energy E . Once particles are binned in a grid of $n_E \times n_x$ energy and circularity cells, we compute the average weight \hat{w}_{kl} ($k = 1, \dots, n_E, l = 1, \dots, n_x$) contained in each cell, and then we assign it as a new prior to all the particles belonging to that cell.

Provided the (E, x) grid correctly resolves the relevant phase-space properties of the target, such new priors ensure an orbit-based regularization which acts locally, homogenizing the weights of particles moving on the same and on neighbouring orbits, but at the same time tolerates global differences among particles on different orbits.

2.3.2 Smoothing of the grid of particle priors

We will see that the priors computed in this way can be quite noisy. To avoid coarseness in the distribution of priors, and so ensure the global smoothness of the underlying model DF represented by the (E, x) grid, we implement a two-dimensional spline fit of the gridded priors. The technique (Press et al. 1992) is well known and widely used, also in an astrophysical context (*e.g.* Merritt 1993; Gerhard et al. 1998; Das et al. 2010): a thin-plate spline function for the new priors on the grid is searched, that minimizes the penalized least square function

$$\Delta^2 \equiv \sum_{k,l} \xi^2 + \lambda \sum_{k,l} \Lambda(\hat{W})_{kl}, \quad (9)$$

having defined a function $\hat{W}(E, x)$ which equals the values of the priors on the (E, x) grid. In the equation above, ξ^2 measures the deviation between the original value of the

prior and its spline value in each (k, l) -cell, and

$$\Lambda(\hat{W})_{kl} = \left[\left(\frac{\partial^2 \hat{W}}{\partial E^2} \right)^2 + 2 \left(\frac{\partial^2 \hat{W}}{\partial E \partial x} \right)^2 + \left(\frac{\partial^2 \hat{W}}{\partial x^2} \right)^2 \right]_{\substack{E=E_k \\ x=x_l}} \quad (10)$$

quantifies the complexity of the fitting spline in terms of the second derivatives, which are numerically computed via finite differences.

The regularization parameter λ determines which of a family of splines, ranging from a plane for $\lambda \rightarrow \infty$ to an interpolating cubic spline surface for $\lambda \rightarrow 0$, is fitted to the grid of priors. Obviously, the optimal λ is that which resolves the relevant structures in the underlying prior distribution, but at the same time damps strong and presumably spurious variations among nearby priors.

In principle, λ can be calibrated with a sequence of experiments on the (E, x) grid. However, since particle weights evolve in time, and so does the grid of priors, we decided to implement the General Cross Validation technique (GCV, Wahba 1990) to determine automatically the optimal value of λ each time a new grid of priors is computed. GCV is based on the principle of sequentially omitting each data point, re-fitting the spline, and predicting the value of the point from the spline. The technique singles out the optimal value of λ for this to work best.

2.3.3 New definition of pseudo-entropy

The new moving priors substitute the traditional ones in the definition (8) of the pseudo-entropy, which we slightly modify in order to account for the normalization of the weights. As already noted, maximizing the standard entropy biases the weights towards \hat{w}_i/e , so that oversmoothing (*e.g.* for high values of μ) causes an undesired global decrease of all weights which leads to a poor fit of the mass distribution (see *e.g.* Fig. 10 in DL08).

In order to avoid such problems, we define a new weight entropy

$$S = - \sum_{i=1}^N w_i \left[\log \left(\frac{w_i}{\hat{w}_i} \right) - 1 \right], \quad (11)$$

for which we can immediately check that (i) maximizing this quantity pushes the weights to the actual values of the priors, (ii) positive and negative corrections to the weights are now a priori equally likely, and (iii) the whole regularization scheme is neutral to mass, so that the only power to alter the total mass of the system is left to the data, see Section 3.2.

3 TARGET MODELS AND OBSERVABLES

In this Section we construct a series of spherical targets to be modelled with NMAGIC (Section 4 and 5) in order to address two issues, namely (i) testing the ability of the new regularization scheme to fit the target data with an intrinsically smooth and unbiased particle model, and (ii) exploring the extent to which the χ^2 M2M technique can recover the target phase-space structure from a given data set independently of the initial particle model.

With these aims in mind, we first focus on a problem whose solution is theoretically known to be unique. As

proved by Dejonghe & Merritt (1992) in the spherical non-rotating case, if the gravitational potential is known and complete information on the LOSVD at all radii is available, then the underlying DF can be uniquely recovered. Therefore, the first target model we design has a known spherical potential and is truncated in radius, so that photometric and kinematic data can fully constrain it.

As a second target model, we build an untruncated (infinite) system whose outer regions remain unconstrained by data, similar to the case of modelling real galaxies.

For both target models, we use the 3D luminosity density together with the LOSVD along several long-slits as target data in the modelling, similar to DL08 and DL09. For each model, we generate both a set of idealized kinematic data, i.e. a large number of data points with small error bars, and a set of more realistic, i.e. sparser and noisier, data points. We use NMAGIC itself to construct our target dynamical equilibrium structures, and to determine their observables, as described in more detail in the following subsections.

3.1 Spherical anisotropic Hernquist targets

Our target models are Hernquist (1990) spheres with a radially anisotropic orbital structure either of the Osipkov-Merritt kind (Osipkov 1979; Merritt 1985, hereafter OM), or of the more mildly anisotropic, quasi-separable kind (Gerhard 1991). Generally speaking, they are isotropic in the central regions, and radially anisotropic for radii greater than a specified anisotropy radius.

The potential-density pair for Hernquist models is

$$\rho(r) = \frac{aM}{2\pi r(r+a)^3}, \quad \varphi(r) = -\frac{GM}{r+a}, \quad (12)$$

where M is the total mass, G the gravitational constant and a the scale length. We set the scale length equal to 1 kpc, and we use characteristic values of the elliptical galaxy NGC 3379 for the total luminosity $L = 1.24 \times 10^{10} L_{\odot}$, the stellar mass-to-light ratio $\Upsilon = 5$, and the distance $D = 9.8$ Mpc. The projected effective radius of our target model is $R_{\text{eff}} \approx 38.3'' = 1.82$ kpc.

With respect to the orbital anisotropy, we either fix the OM anisotropy radius $r_a = 2a$, or we use $\alpha = 2$ and $L_0 = 0.3\sqrt{GMa}$ in the prescription of Gerhard (1991) to generate moderately radially anisotropic models (see equations [2.2] and [3.14] therein).

Following the method described in Debattista & Sellwood (2000), we generate particle model realizations of the spherical targets. To construct a truncated target, we only retain particles with energies lower than $E_{\text{max}} \equiv \varphi(r_{\text{max}})$, with r_{max} equal to the model boundary.

Finally, we relax the particle models in the fixed Hernquist potential (note that the truncated target is therefore not a self-consistent system), and we compute the target observables from the final particle model using NMAGIC to integrate the particles, as detailed below.

3.2 Luminosity observables

We consider as density constraint a spherical harmonics expansion of the target luminosity density on a 1-D mesh of

radii r_k . The expansion coefficients

$$a_{lm,k} = L \sum_i \gamma_{ki}^{CIC} Y_l^m(\theta_i, \varphi_i) w_i \quad (13)$$

are computed from the particle realizations through NMAGIC, making use of the cloud-in-cell technique (see *e.g.* DL07, Binney & Tremaine 2008) to distribute the weight of a particle between nearby grid points. In the definition above, L is the total luminosity of the target, Y_l^m are the standard spherical harmonic functions, and γ_{ki}^{CIC} is the selection function associated with the cloud-in-cell scheme. The radial grid has 60 points, quasi-logarithmically spaced between $r_{\text{min}} = 0.01''$ and r_{max} equal to the model boundary (for the truncated target) or to $1500'' \sim 40R_e$ (for the infinite target).

Poissonian error bars, dependent on the number of particles in each shell, are assumed for the radial mass, while 50 Monte-Carlo realizations of the density field of the target model allow errors to be assigned to the higher order mass moments (see DL07). Because the targets are spherical, all model $a_{lm,k}$ with $l \neq 0, m \neq 0$ are constrained to be zero within these errors, while the $a_{00,k}$ are constrained by their values for the known target luminosity distribution.

When comparing the target data with the model observables, we compute the latter in the exact same way from the particle model.

By fitting the $a_{lm,k}$ coefficients (13), the total luminosity of the model is adjusted to the target luminosity L . The sum of the weights, initially set to $\sum_{i=1}^N w_i = 1$, may therefore change if the luminosity of the initial model $L_{\text{initial}} \neq L$. In this work, we set $L_{\text{initial}} = L$, and we do not adjust the mass-to-light ratio, except in Section 6, so that the total mass is also constant throughout the evolution.

3.3 Kinematic observables

As kinematic target observables, we use the luminosity-weighted Gauss-Hermite moments of the LOSVD (van der Marel & Franx 1993; Gerhard 1993) in various slit cells, computed from the particle realizations using NMAGIC, through

$$b_{n,p} \equiv l_p h_{n,p} = 2\sqrt{\pi}L \sum_i \delta_{pi} u_n(\nu_{pi}) w_i \quad (14)$$

(DL07). Here, l_p is the luminosity in slit cell C_p , δ_{pi} selects only particles belonging to that cell, the dimensionless Gauss-Hermite functions are

$$u_n(\nu) = (2^{n+1} \pi n!)^{-1/2} H_n(\nu) \exp(-\nu^2/2), \quad (15)$$

where H_n denote the standard Hermite polynomials, and finally

$$\nu_{pi} = (v_{z,i} - V_p) / \sigma_p, \quad (16)$$

with $v_{z,i}$ the line-of-sight velocity of particle i , and V_p and σ_p the best-fitting Gaussian parameters of the target LOSVD in the given slit cell.

To compute V_p, σ_p, h_3, h_4 from the particle model, we adopt the following procedure. First, we compute the mean velocity and rms velocity of particles in each slit cell, and use them to estimate the $b_{n,p}$ from the particles through equations (14). Next, we use the first order relations

$$\Delta h_1 = -\frac{1}{\sqrt{2}} \frac{\Delta V}{\sigma}; \quad \Delta h_2 = -\frac{1}{\sqrt{2}} \frac{\Delta \sigma}{\sigma} \quad (17)$$

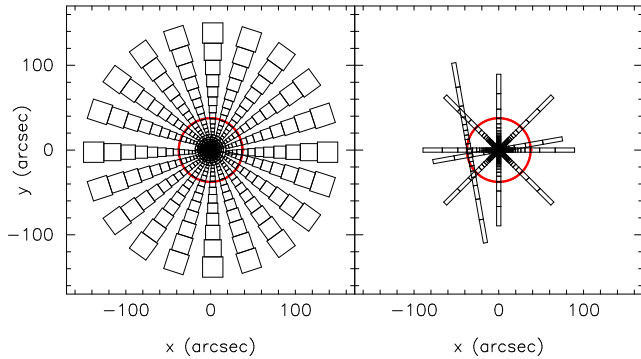


Figure 1. Geometry of the two different slit setups. The red circle corresponds to R_{eff} . *Left panel:* idealized configuration of 10 slits covering the target; slit cells outside $R_{\text{eff}}/2$ are square (see Section 3.3). *Right panel:* realistic slit configuration, adapted from NGC 3379 (DL09).

(van der Marel & Franx 1993; Rix et al. 1997) iteratively to correct V_p and σ_p , until h_1 and h_2 both converge to zero. Then, the new target moments $b_{n,p}$ are temporally smoothed to reduce fluctuations caused by particle noise, and this leads to values of h_1 and h_2 slightly different from zero. Finally, the resulting velocity profile is fitted by a Gauss-Hermite series (van der Marel & Franx 1993) setting $h_1 = h_2 = 0$, and the $b_{n,p}$ are recomputed.

Two different slit configurations are considered, as shown in Fig. 1. There, the left panel illustrates a schematic view of an idealized slit data setup, which consists of 10 slits covering the target and extending as far as $r_{\text{max}} = 150'' \sim 4R_{\text{eff}}$. In order to increase spatial coverage in the outer regions, and so to decrease the effects of particle noise, slit cells outside $R_{\text{eff}}/2$ are enlarged and made square. Moreover, Gauss-Hermite coefficients up to h_6 are considered. To assign error bars to the target kinematic data, we compute averaged values of the final time-smoothed $b_{n,p}$ moments in the 10 different slits, and then we set the errors equal to $\sqrt{2}$ times the rms deviation of the individual slit cell moments from the average¹. To complete the generation of this slit data set, Gaussian random variates with 1σ equal to these errors are added to the average moments $b_{n,p}$. In the following, we refer to this kinematic data set as *idealized* data.

For the truncated model, these data are sufficiently close to the required “complete” data set that we would expect to be able to recover the theoretically unique underlying model with very good accuracy.

The right panel of Fig. 1 shows instead the 6 slits which were used by DL09 to model NGC 3379; for this second slit configuration, $r_{\text{max}} = 100'' \sim 3R_{\text{eff}}$, only v, σ, h_3, h_4 are available, and observational errors for this galaxy are adopted. Finally, Gaussian random variates are added to the data with 1σ equal to the observational errors. Hereafter we refer to this latter kinematic data set as *realistic* data.

¹ The factor $\sqrt{2}$ in the error bars is necessary because, given this generation of kinematic data, the NMAGIC model will have an intrinsic particle noise similar to that of the data which it will try to match.

4 CONVERGENCE TO A THEORETICALLY UNIQUE SOLUTION

Here we construct NMAGIC models for the radially anisotropic target galaxy model described above. As constraints we use the luminosity density and the *idealized* kinematic data. We determine the amount of regularization, investigate whether it is possible to converge to the theoretically unique solution, and see how well the target galaxy can be reproduced starting from different initial particle models.

Our NMAGIC models show for this case that if a unique inversion of data to recover the underlying target DF exists, then it can actually be found via χ^2 M2M modelling from good enough data. The new regularization method proposed in this paper significantly improves both the accuracy with which the target intrinsic properties are reproduced, and the convergence to the right solution independently of initial conditions.

4.1 Modelling procedure and diagnostic quantities

Starting from an initial particle model, the weights of all particles are evolved until the particle system matches the target. As initial particle system, we adopt an isotropic Hernquist sphere with the same luminosity but scale length $a = 1.5$ kpc. Different velocity distributions are also considered, as specified below. During the whole evolution, the potential is kept fixed to the target potential. The particles are integrated using a leap-frog scheme.

After a relaxation phase in which the particle system is advanced without weight correction, weights are updated according to the force-of-change in equation (4), i.e. subject to both data constraints and smoothing constraints, for $\sim 10^5$ correction time steps. We define the model to have converged if χ^2/J averaged over 50 steps is almost constant in the last 10^4 steps, with fluctuations which are typically of order 2%. The particle weights are then constant to a similar accuracy with MPR. Finally, the particles are freely evolved for another 10^4 steps without any further weight correction, to ensure that the final particle model is well phase-mixed. For reference, 10^4 correction time steps correspond to ~ 42 circular rotation periods at the target R_{eff} .

When using the new regularization scheme, individual priors are not kept constant in time but rather they are continuously updated while particle weights are changed to match the target observables, as detailed in Section 2.3. Particles are sorted according to their orbital integrals in a grid of $n_E = 30$ and $n_x = 10$ bins, chosen as a compromise between retaining good resolution for the orbit distribution and ensuring a sufficient number of particles in all grid cells. The average weight contained in each grid cell is computed, and then a GCV thin-plate smoothing spline is fitted to the distribution of average weights on the grid. The spline value in every grid cell is finally assigned as the new prior to all particles belonging to the cell.

A typical outcome of the procedure early in the evolution is shown in Fig. 2, where the (E, x) grid of priors is plotted before (left) and after (right) smoothing, and similarly for a horizontal cut (fixed angular momentum) through the grid. The cut shows considerable noise before smoothing in the central grid cells, where even with a total $N \sim 10^6$ particles the number of particles per cell for a Hernquist

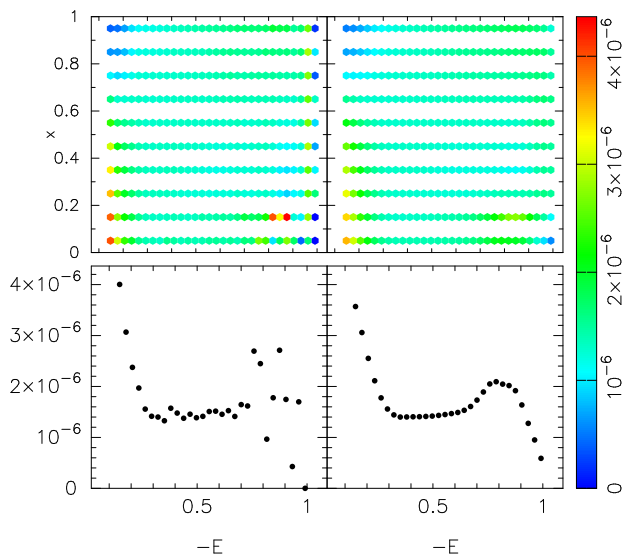


Figure 2. Top: unsmoothed (*left*) and smoothed (*right*) grid of individual particle priors after $\sim 10^3$ correction time steps (colour bar on the right). Bottom: a cut of the above grid for $x = 0.05$, showing unsmoothed (*left*) and smoothed (*right*) particle priors as a function of energy. Priors are smoothed among nearby cells with the GCV thin-plate smoothing spline described in Section 2.3.2.

model cusp is still small. In the tests presented here, new priors are computed frequently in the initial phase and every 10^4 correction time steps later in the run, which results in an efficient regularization at a minimum computational cost. When testing the new scheme for very large μ values, priors are computed and updated more often.

The quality of the final particle model of each run is assessed through three diagnostic quantities. The first is the goodness of the fit to the data in terms of χ^2/J , where J is the number of data points. Assuming the goodness of fit statistics follows a χ^2 probability distribution function, the mean of the χ^2 distribution is equal to the number of degrees of freedom, i.e. the number of constraints (data points plus constraints introduced by the merit function) subtracted by the number of parameters (model parameters plus fitted weights), which are both difficult to quantify. However, if the number of degrees of freedom is approximately equal to the number of data points, then $\chi^2/J < 1$ means that we are fitting the data well.

The second is the level to which the known intrinsic kinematics of the target galaxy are recovered by NMAGIC, quantified by the rms difference between the intrinsic velocity moments of the target galaxy and those of the final particle model realization. In the following, the internal kinematics (streaming velocity and velocity dispersions) of the particle model are computed by binning particles in spherical polar coordinates, using 21 radial shells quasi-logarithmically spaced between $r_{\min} = 0.01''$ and r_{\max} , 12 bins in the azimuthal angle ϕ , and 21 equally spaced bins in $\cos \theta$, where θ is the polar angle.

Finally, we determine the degree to which the particle model reproduces the known phase-space structure of the spherical target. To quantify this we compute the mass-weighted relative rms difference between model and target weights ($w_{kl,m}$ and $w_{kl,t}$, respectively) in the grid of energy

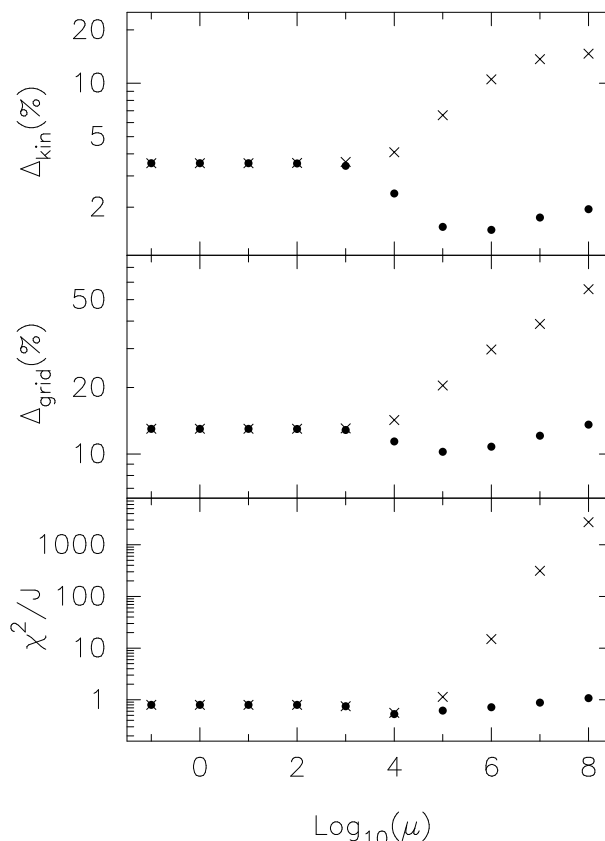


Figure 3. Quality of the final NMAGIC particle models as a function of the regularization parameter μ . *Top panel:* rms deviation (%) of the final particle model from the target internal velocity moments. *Middle panel:* rms deviation (%) between the occupation of the (E, x) grid of the target and of the final NMAGIC model. *Bottom panel:* goodness of the particle model fit to photometric and kinematic data. Crosses refer to models obtained with the traditional GWR scheme, dots to models obtained with the new MPR.

and circularity (E, x) used also for the regularization:

$$\Delta_{\text{grid}} = \sqrt{\frac{\sum_{k,t} w_{kl,t} \left(\frac{w_{kl,t} - w_{kl,m}}{w_{kl,t}} \right)^2}{\sum_{k,l} w_{kl,t}}} \quad (18)$$

4.2 Calibrating regularization

Following the same approach as Gerhard et al. (1998), Thomas et al. (2005), DL08, and DL09, we construct NMAGIC models for the target galaxy which only differ in the adopted regularization scheme and the amount of regularization, i.e. the value of the parameter μ . Note that ε is kept constant between all models.

The results are summarized in Fig. 3, where the normalized goodness of fit χ^2/J , the mass-weighted rms over the (E, x) grid, Δ_{grid} , and finally the rms difference between the internal velocity moments of the target and final particle model, Δ_{kin} , are plotted as a function of μ , from unsmoothed models (small μ) to oversmoothed models (high μ).

We first focus on the NMAGIC particle models obtained with the traditional GWR technique (crosses, Fig. 3). For a wide range of values of $\mu \leq 10^4$, NMAGIC is able to fit the data with $\chi^2/J \lesssim 1$. No clear minimum is present in the

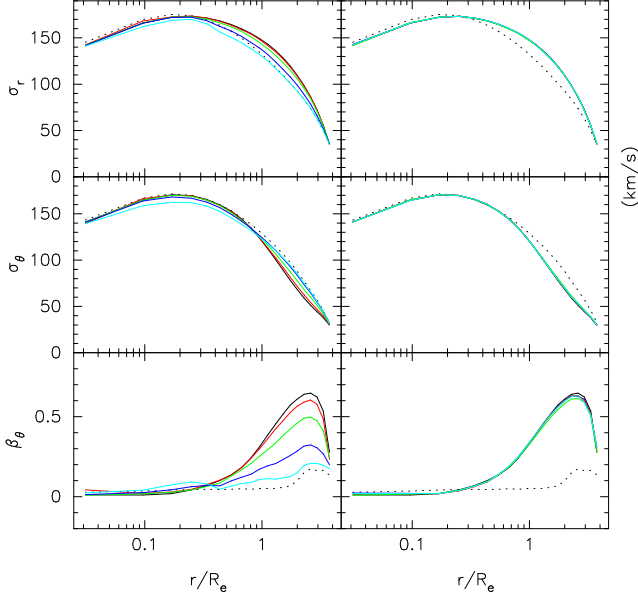


Figure 4. Intrinsic kinematics of the NMAGIC models obtained with the GWR (*left panel*), and with the new MPR method (*right panel*). From top to bottom: radial velocity dispersion profile, vertical velocity dispersion profile, and anisotropy parameter. The dotted and full black lines show the intrinsic kinematics of the initial near-isotropic particle model, and of the truncated target galaxy, respectively. Red, green, blue, and light blue lines correspond to $\mu = 10^3, 10^4, 10^5, 10^6$ adopted in the modelling (see Section 4.2).

plotted rms deviations in grid and intrinsic kinematics as a function of μ : these quantities stay almost flat for a large range of μ , and then rapidly increase for $\mu \gtrsim 10^4$, when the increasing amount of smoothing upsets the fit to the data. By the time the smoothing becomes effective in damping fluctuations in the intrinsic quantities, the bias introduced by the global nature of the smoothing has already set in - hence no clear optimal value of μ is found. For GWR and this particular data set, $\mu = 10^4$ gives a good compromise between quality of the data fit and recovery of the target properties - but with little smoothing.

How well the intrinsic kinematics of the target galaxy can be recovered is shown in the left panel of Fig. 4, which compares the known target kinematics with the final NMAGIC models obtained with $\mu = 10^4, 10^5, 10^6, 10^7$. As expected, for higher values of μ the internal moments remain closer to the initial isotropic moments.

Fig. 5 shows the level to which the known target DF can be recovered by NMAGIC for $\mu = 10^4, 10^6$: the distribution of total particle weights in the (E, x) grid is plotted for the initial particle model, the truncated target, and the models obtained with NMAGIC. We denote this by “mass distribution function”, or MDF for brevity. Clearly, for $\mu = 10^4$ the main phase-space structures are well recovered, showing that NMAGIC is able to fit the data and to approximately find the underlying MDF, but the peak on high- E near-radial orbits is underestimated because of the global nature of GWR. For the more heavily smoothed case with $\mu = 10^6$, this peak is completely wiped out.

We now consider χ^2 M2M models obtained by fitting the same target data with MPR. As can be seen in Fig. 3

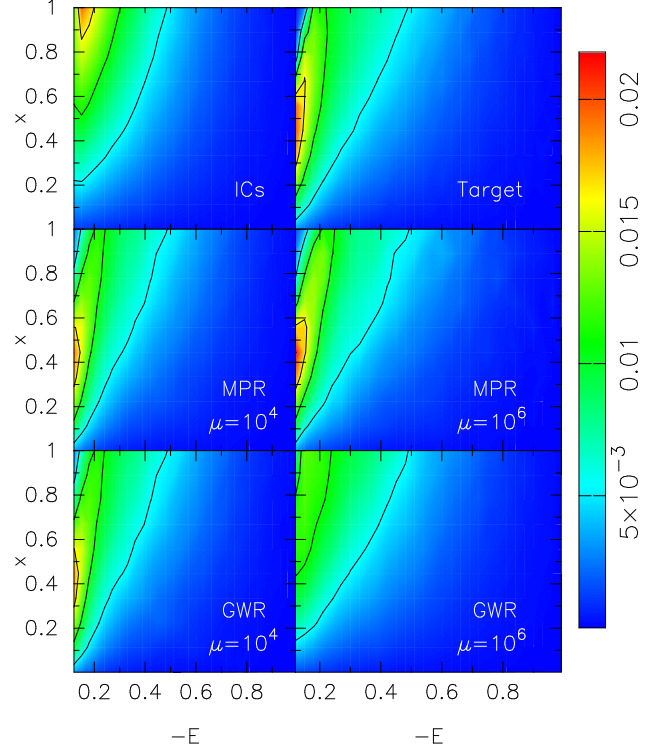


Figure 5. Mass distribution function (MDF) of particle weights in the (E, x) grid, for the initial particle model (top left), the truncated target galaxy (top right), the models obtained with the standard GWR (bottom) and with the MPR method (middle), for different values of μ . The colour scheme reflects the total weight contained in each grid cell, where $n_E = 30$, $n_x = 10$.

(black dots), the new method works very well in reproducing the target, and a series of NMAGIC models fitting the photometric and kinematics constraints of the galaxy within $\chi^2/J \lesssim 1$ can be generated for a wider range of μ values. Of these, models obtained for values of $\mu \lesssim 10^3$ are essentially driven by the χ^2 term alone. However, when regularization becomes significant, a minimum is reached both in the rms deviation between intrinsic moments of the particle model and of the target, and in the rms deviation of their (E, x) distributions (top and middle panels of Fig. 3, respectively). Remarkably, the minimum is well below that achievable with traditional weight entropy smoothing, indicating that the phase-space structure and the internal moments of the target can be recovered much better using MPR.

The right panel of Fig. 4 shows how close the internal kinematics of the final particle models for $\mu = 10^4, 10^5, 10^6, 10^7$ are to those of the target galaxy. Note that the residuals are so small that the trend with μ seen in Fig. 3 cannot be seen; the new scheme allows one to recover the target moments almost perfectly. The accuracy with which the MDF in (E, x) integral space is reproduced is shown in Fig. 5. Visually comparing this plot with the corresponding ones for the truncated target and the best model obtained using standard GWR, shows that the target is now recovered much better. In particular at small energies, i.e. in the outer regions, the weight of particles on radial orbits is increased while that of particles on circular orbits is decreased more effectively with MPR, especially for the preferred $\mu = 10^6$.

We conclude that, for this particular data setup, the

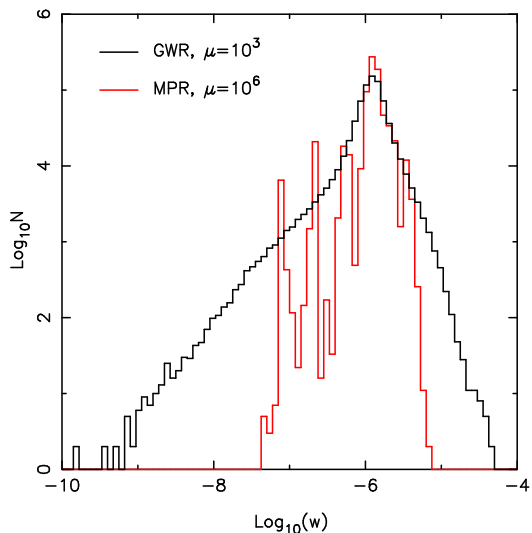


Figure 6. Distribution of particle weights for the final optimally smoothed NMAGIC models obtained with the traditional GWR (black histograms, $\mu = 10^3$) and with the MPR scheme (red histograms, $\mu = 10^6$). Particle weights were initialized to $w_0 = 1/750000 \sim 10^{-6}$.

best choice for μ with MPR is $\sim 10^6$. This value is considerably larger than the corresponding μ of the traditional GWR, showing that the new regularization succeeds better in reconciling the smoothness of the underlying model with orbital anisotropy.

It is instructive to compare the final distribution of particle weights for both regularization schemes. Fig. 6 shows that MPR results in a more compact and more structured weight distribution, which avoids extended tails of extremely increased or decreased weights, while still providing a good and less noisy fit the data (see below). A similar comparison in the context of Schwarzschild modelling can be found in Fig. 17 of Thomas et al. (2007).

Along with a more compact weight distribution, MPR also leads to a smoother particle model. This can be quantified by computing the rms fluctuations of particle weights around the mean value in all the cells of the (E, x) grid for the different kinds of regularization, as shown in Fig. 7.

Not unexpectedly, the fit to the data also looks smoother when adopting the new regularization, and the larger μ value permitted by this scheme opposes an overfitting of the data points, as can be appreciated for different observables in Section 6.

To summarize, we have tested the χ^2 M2M method with a new Moving Prior Regularization scheme for a radially anisotropic truncated target model with *idealized* data, and have calibrated the best value of the regularization parameter μ . We have shown that the corresponding NMAGIC models match the target data well and recover the MDF for this model in its known potential. We have also seen that these models are much less sensitive to the value of μ than with the traditional weight entropy regularization, which can only reproduce the global anisotropy of this model essentially without smoothing. The new regularization scheme allows NMAGIC to recover a particle model that fits the data well but is both intrinsically smoother and reproduces the properties of the target more accurately.

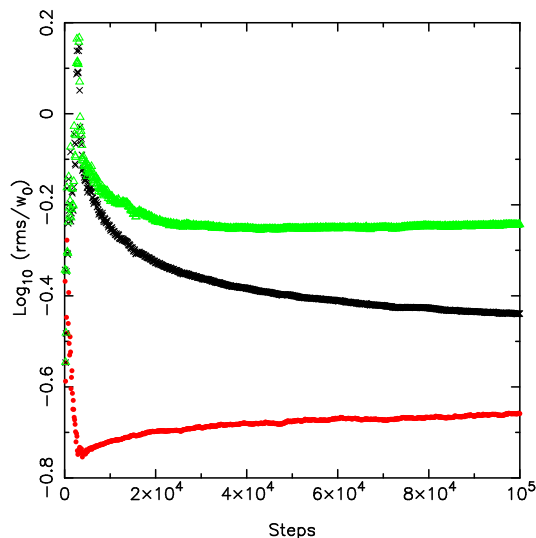


Figure 7. Rms fluctuations of particle weights around the mean value in each (E, x) cell for the optimally smoothed NMAGIC models obtained with GWR (black crosses, $\mu = 10^4$) and with MPR (red dots, $\mu = 10^6$), as a function of the number of NMAGIC correction time-steps. The top curve (green triangles) shows an essentially unsmoothed model ($\mu = 10^3$). $w_0 = 1/750000 \sim 10^{-6}$ is the value of the initial particle weights. The grid has $n_E = 30$ times $n_x = 10$ cells, and only those containing more than 50 particles are taken into account, to avoid particle noise effects in the computation of the residuals.

4.3 Varying the initial particle model

The results of the previous subsection already show that NMAGIC can recover the orbit distribution of our truncated spherical target galaxy from a set of data that specifies it essentially uniquely. In this experiment, we used an isotropic initial model, so now we investigate the natural question whether and how this result is dependent on the choice of initial particle model.

In particular, we consider both the case in which the initial particle model has a radially anisotropic OM orbital structure (with anisotropy radius $r_a = 3a$, different from the target galaxy), and the case in which it is tangentially anisotropic according to the quasi-separable prescription of Gerhard (1991, with $\alpha = 2$, $L_0 = 0.3\sqrt{GMa}$, $c = 0.1$). For both initial particle models we checked that a minimum number of particles on radial and tangential orbits is present at each energy. By analogy with the experiment described in the previous subsection, the initial particle models are Hernquist spheres with scale-length $a = 1.5$ kpc, larger than the target galaxy ($a = 1$ kpc). The same setup of the NMAGIC run is adopted, together with the optimal μ values determined in Section 4.2 above for the two regularization methods.

With the new MPR scheme, the final NMAGIC models obtained for different initial orbital distributions differ remarkably little. Table 1 and Figs. 8-9 show how well the intrinsic kinematics and phase-space MDF match those of the known target galaxy. The MDF of the final particle model is very similar to that of the target galaxy, independent of the choice of initial conditions (Fig. 9). Typical fluctuations in the mass-weighted relative rms difference between target

		ICs	χ^2/J	$\Delta_{\text{kin}}(\%)$	$\Delta_{\text{grid}}(\%)$
<i>Idealized</i> data	GWR	iso	0.57	4.07 (14.67)	14.24 (43.98)
		rad	0.46	3.62 (11.85)	12.94 (32.25)
		tang	1.64	7.56 (27.20)	17.51 (75.46)
	MPR	iso	0.72	1.49 (14.67)	10.80 (43.98)
		rad	0.67	1.62 (11.85)	11.21 (32.25)
		tang	1.57	3.38 (27.20)	12.53 (75.46)
<i>Realistic</i> data	GWR	iso	0.26	2.44 (5.17)	7.49 (17.63)
		rad	0.20	3.25 (3.85)	12.68 (15.79)
		tang	0.29	7.42 (16.14)	20.85 (56.44)
	MPR	iso	0.37	1.32 (5.17)	7.39 (17.63)
		rad	0.38	3.13 (3.85)	10.27 (15.79)
		tang	0.38	2.35 (16.14)	11.09 (56.44)

Table 1. NMAGIC models for the truncated target galaxy. Different initial particle models are adopted. For the traditional weight entropy smoothing $\mu = 10^4$; for the new regularization scheme, $\mu = 10^6$. The goodness of fit χ^2/J , Δ_{kin} and Δ_{grid} are computed as described in Section 4.1. In brackets, the same Δ_{kin} and Δ_{grid} computed between the initial particle model and the target.

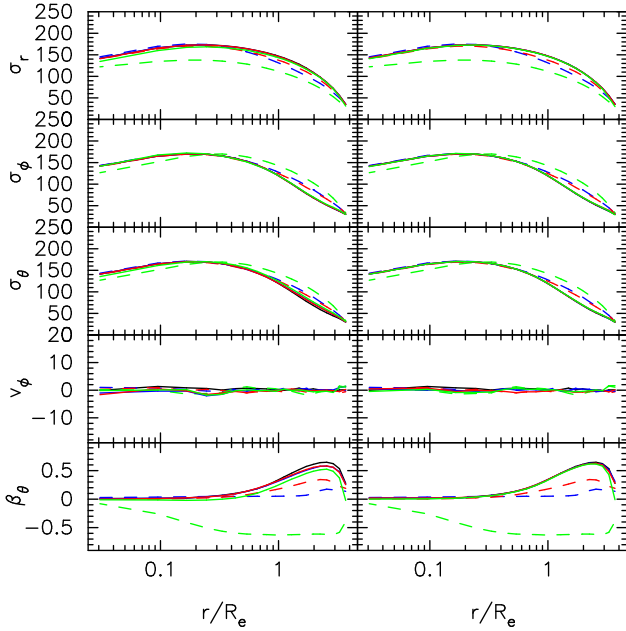


Figure 8. Truncated target with *idealized* data: recovery of the intrinsic kinematics with different initial particle models. From top to bottom: radial, azimuthal, and vertical velocity dispersion profiles, mean azimuthal streaming velocity, and anisotropy parameter of the NMAGIC models (full lines) for different initial conditions (dashed lines). The black line indicates the intrinsic moments of the target galaxy. Blue, red and green colours correspond to isotropic, radially anisotropic and tangentially anisotropic initial conditions, respectively. GWR was adopted in the runs shown in the *left panel*, while MPR in the runs shown in the *right panel*.

and model MDF are 12%, while the intrinsic kinematics of the target is recovered almost perfectly, as shown in Fig. 8.

It is instructive to see how a similar result cannot be achieved with the traditional weight entropy: an inspection of Table 1, or Fig. 8 and Fig. 9 shows the poorer accuracy of the resulting particle models. Especially for the models with tangentially anisotropic initial conditions, the smaller

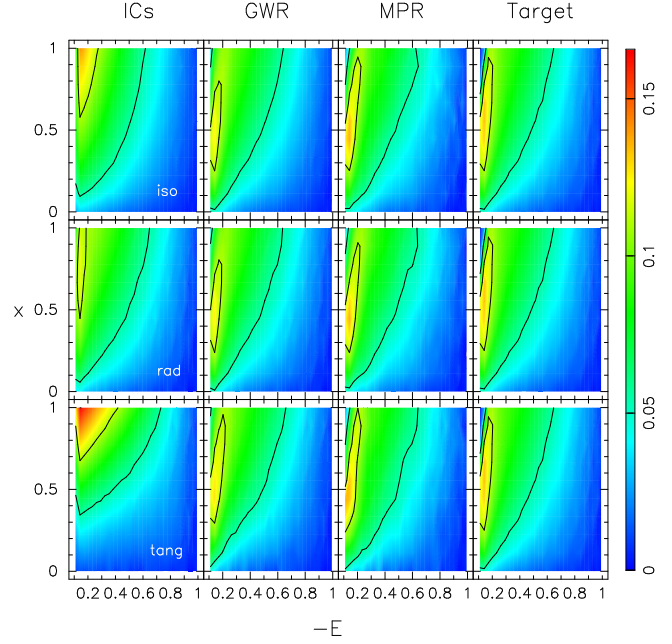


Figure 9. Recovery of the MDF of the truncated target (last column on the right) for different initial particle models from *idealized* kinematic constraints. The first column shows the distribution of particle weights in the (E, x) grid for the isotropic, radially and tangentially anisotropic initial particle models (from top to bottom). The second column corresponds to the final NMAGIC particle models obtained with traditional GWR; the third column to the models obtained using the new MPR. The colour scheme reflects the square root of the total weight contained in each grid cell, where we have adopted $n_E = 30$, $n_x = 10$.

number of particles on radial orbits together with GWR makes it more difficult to reproduce the radially anisotropic target.

We conclude that with the new regularization method NMAGIC converges to the (theoretically essentially unique) solution to a very good level of accuracy, independently of the choice of the initial particle model. In this respect, the new MPR method is a definite improvement over the traditional weight entropy scheme.

5 EFFECTS OF IMPERFECT DATA

In astronomical applications, the data constraints are typically less stringent than in the idealized case considered so far. We therefore now investigate how the results change in more realistic circumstances.

The following tests represent a sequence of problems that are increasingly less determined by the data, starting from the truncated target covered by *realistic* data (Sec. 5.1), and moving on to infinite stellar systems constrained by data with finite extent. This allows us to isolate the different roles played by the quality and completeness of data, the initial particle model, and the regularization scheme.

We find that it is still possible to get close to the target dynamical structure from different initial particle models with the help of the new regularization method, even though

the lack and/or poor quality of data introduce degeneracies in the models.

5.1 Truncated target and realistic kinematic errors

First we construct NMAGIC models for a truncated target with the *realistic* kinematic data, with the goal to establish how well the target galaxy can then be reproduced from different initial particle systems.

The *realistic* data have larger error bars and smaller data coverage (see Section 3.3). For these models $r_{\max} = 100''$ is thus smaller than in the previous case. The different initial particle models have the same anisotropy structure as in Section 4.3, but are adapted to this r_{\max} - hence they are more similar to the target.

We have repeated the analysis described in Section 4.2 to determine the optimal value of the smoothing parameter μ when these *realistic* data are adopted. Results do not change much, and suggest that we can keep the values of $\mu = 10^4$ for the GWR and $\mu = 10^6$ for MPR.

The results of these models are shown in Figs. 10 (top part) and 11, and more quantitatively in Table 1, for both regularization methods. The top part of Fig. 10 shows the deviations of the models from the target, comparing the two cases in which *idealized* and *realistic* constraints are used. The three subpanels show the deviations of $\sigma_r^2 - \sigma_\theta^2$ and $\sigma_\phi^2 - \sigma_\theta^2$ normalized by the sum of the two velocity dispersions, and the deviations of the velocity anisotropy β , as a function of radius. In this figure, the shaded regions correspond to the range of deviations obtained from modelling the data with the chosen initial particle systems.

As intuitively might be expected, these deviations increase (*i*) moving to larger radii, and (*ii*) when *realistic* data are considered. The effect of imperfect data on the final models is noticeable, in particular closer to the model boundary where poorer constraints from slit data worsen the recovery of the intrinsic kinematics.

However, we see that also for realistic data the new MPR works well in recovering the internal kinematics of the target galaxy independently of the initial particle model, and it is superior to the GWR, as deviations are considerably smaller.

The accuracy with which the phase-space mass distribution function of the target is matched by the NMAGIC models is shown in Fig. 11, where is clear that the traditional GWR works less well with these realistic data, especially when tangential initial conditions are adopted.

Because the realistic error bars are larger than those used in the experiments in Section 4, the particle weights undergo smaller changes until they match target observables in a χ^2 sense [see equations (6) and (7)]. For the same reason, the final normalized χ^2 between data and model observables turns out to be smaller (see Table 1).

To conclude, these experiments show that the new MPR method improves both the quality with which the intrinsic properties of the target galaxy can be recovered, and the independence of the final particle model from the adopted initial model. In fact, MPR makes it possible to recover the underlying dynamical structure of our radially anisotropic target galaxy with good accuracy ($\Delta\beta \sim \pm 0.1$ only at the outermost point) even when the quality of the data is not

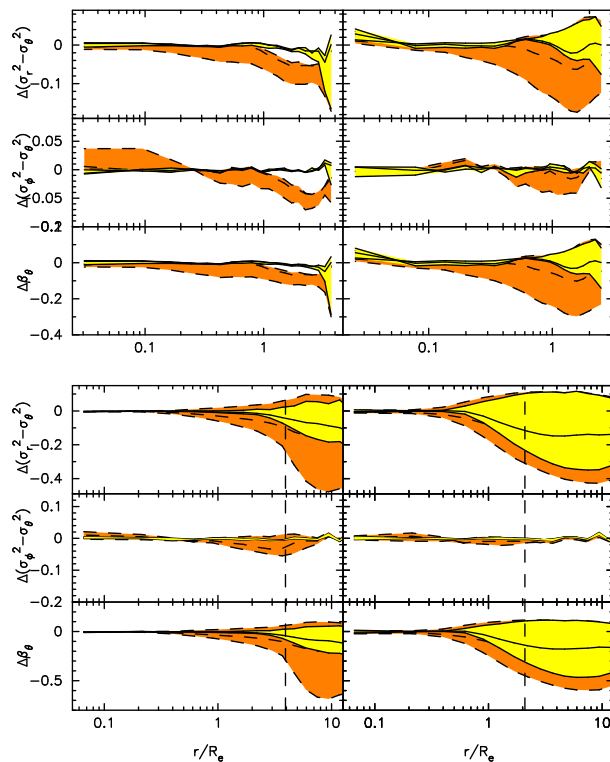


Figure 10. Recovery of the intrinsic kinematics for the truncated and infinite targets (top and bottom figure, respectively) with *idealized* and *realistic* data (left and right columns, respectively). The vertical dashed line corresponds to the radial extent of the data for the infinite target. The shaded yellow (orange) area shows the range of deviations for the MPR (GWR) method, when the specified range of initial conditions is adopted. Full (dashed) lines represent the deviations for the final NMAGIC models obtained with MPR (GWR) starting from different initial particle models. Plotted in each panel are, from top to bottom, deviations of normalized $\sigma_r^2 - \sigma_\theta^2$, $\sigma_\phi^2 - \sigma_\theta^2$, and anisotropy parameter β from the respective true value of the target; see Sections 5.1 and 5.2.

perfect. As already noticed, MPR allows the use of higher μ values, thus reducing mass fluctuations and enforcing the smoothness of the underlying model without spoiling the fit to the data.

5.2 Finite data for an infinite target

Real stellar systems are clearly not as sharply truncated in radius as the target galaxies studied so far, and their outer regions are usually not constrained by the available data. We now come to the more realistic case of modelling an infinite target galaxy using finite data, to explore the limitations that the modelling encounters in this case.

As target galaxy we consider our usual Hernquist sphere with scale length $a = 1$ kpc, but this time without truncation. Because of the extreme behaviour of the OM radially anisotropic systems at large radii, we choose a milder anisotropy for our target galaxy, using the models of Gerhard (1991) with specified circularity function [equations (2.2) and (3.14) therein], which only depend on a constant parameter α , set equal to 2.

Following the same procedure as adopted above, we

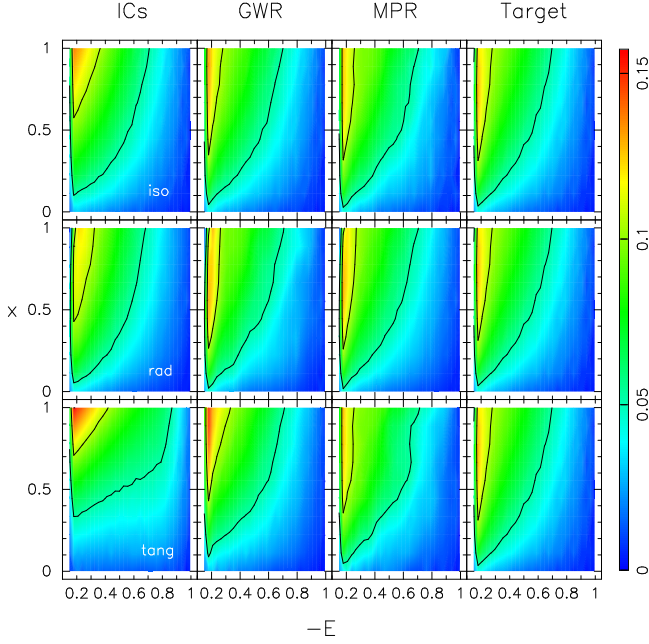


Figure 11. Recovery of the MDF of the truncated target (last column on the right) with *realistic* data for different initial particle models. As Fig. 9.

model the target starting from different initial particle models (isotropic, less radially anisotropic, and more radially anisotropic than the target) and using both regularization schemes. *Idealized* data and *realistic* data are considered in turn.

5.2.1 Infinite target with excellent but radially limited data

Our modelling of the infinite target with *idealized* but radially limited data confirms previous experiments (Thomas et al. 2004, DL08) in that the velocity dispersions, streaming rotation, and anisotropy parameter of the infinite target galaxy can be reproduced reliably only in the regions well inside the part of the galaxy covered by the data.

Quantitative results are reported in Table 2, while the bottom left panel of Fig. 10 shows the range of deviations of the final models from the target obtained for different initial particle systems. The vertical dashed line corresponds to the outermost data point. This panel shows that in the inner regions of the galaxy, where the data provide good constraints to the models, the intrinsic properties of the target galaxy are well recovered independently of the initial particle model, as already found for the truncated target galaxy. However, at larger radii, and close to the outermost data point, regularization plays a dominant role in the weight correction of particles, and in those external regions a bias towards the dynamical structure of the initial particle model cannot be avoided.

Nevertheless, our experiments show that the new MPR considerably reduces such bias towards the dynamical structure of the initial particle model, as can be seen comparing the two shaded regions for MPR and GWR.

If we require $|\Delta\beta| \leq 0.1$ and compute how far out this is achieved for the range of models obtained starting from different initial conditions, we find that this radius is $1.4R_{\text{eff}}$

	ICs	χ^2/J	$(\chi^2/J)_{\text{A1m}}$	$(\chi^2/J)_{\text{slit}}$	
<i>Idealized</i> data	GWR	iso	1.08	0.39	1.17
		$\alpha = 1$	1.02	0.27	1.11
		$\alpha = 3$	0.89	0.21	0.98
	MPR	iso	0.92	0.45	0.98
		$\alpha = 1$	1.02	0.34	1.12
		$\alpha = 3$	0.78	0.34	0.86
<i>Realistic</i> data	GWR	iso	0.54	0.27	0.67
		$\alpha = 1$	0.46	0.19	0.59
		$\alpha = 3$	0.43	0.16	0.56
	MPR	iso	0.62	0.27	0.79
		$\alpha = 1$	0.58	0.25	0.74
		$\alpha = 3$	0.55	0.22	0.71

Table 2. NMAGIC models for the infinite target galaxy in its fixed potential. Different initial conditions and regularization schemes are adopted, as explained in Section 5.2. χ^2 is the usual goodness of fit, normalized by the respective number of observables.

for GWR, while it shifts to $4.3R_{\text{eff}}$ when adopting MPR. Considering instead the radius $r(\Delta\beta = \pm 0.2)$, the standard GWR fails at $3.1R_{\text{eff}}$, while the new method at $8R_{\text{eff}}$.

When, as in this case, a range of dynamical models obtained from different initial particle models is compatible with the data, one could compare and rank models according to the usual goodness-of-fit basis (see *e.g.* Table 2), or additionally according to a plausibility criterion that, *e.g.*, favours a constant or smooth outer anisotropy profile.

5.2.2 Infinite target with realistic and finite data

As a logical final step, we consider the case in which an infinite target like the one described above is constrained by realistic, rather than idealized, data.

We model this target starting again from different initial particle models, and show the accuracy of the final NMAGIC models in the bottom right panel of Fig. 10, and in Table 2.

The bottom part of Fig. 10 compares the deviations of the final models from the target for *idealized* and *realistic* data. Apparently, the realistic constraints on an infinite target galaxy make it really hard for NMAGIC to recover the true intrinsic kinematics of the target independently of the initial particle model, even though it is still true that the new MPR method is superior to the GWR.

To quantify how well the particle model reproduces the intrinsic kinematics of the target galaxy, we can compute $r(\Delta\beta = \pm 0.1)$, which is $0.6R_{\text{eff}}$ for the standard GWR, and $1R_{\text{eff}}$ when adopting the new regularization. Considering instead the radius $r(\Delta\beta = \pm 0.2)$, GWR fails at $0.9R_{\text{eff}}$, while MPR at $1.4R_{\text{eff}}$. Here the kinematic data extend to $\sim 2R_{\text{eff}}$.

Thus, the results previously obtained for the *idealized* data are confirmed: the new regularization scheme provides a better reconstruction of the target properties, and is more independent on the choice of the initial particle model. However, as soon as there is a lack of data to constrain the models, regularization becomes the dominant term in the force of change acting on particle weights, and the bias towards the initial particle model becomes evident.

The main conclusion from these tests is that the reliability of our dynamical models is limited to those regions

in which good observational data exist, and that the better quality of the data is reflected in a better recovery of the intrinsic properties of the target galaxy.

6 REGULARIZED PARTICLE MODELS FOR NGC 4697 AND NGC 3379

We now show our new regularization method at work on two real galaxies, and reconstruct the best-fitting NMAGIC models determined in DL08 and DL09 for the two intermediate luminosity elliptical galaxies NGC 4697 and NGC 3379, respectively.

DL08 and DL09 used NMAGIC to fit spherical and axisymmetric models of different inclinations to extensive data sets for these galaxies, including photometry, long-slit spectroscopy, integral-field data and PNe velocities. Different from the experiments of Sections 4 and 5, particles are evolved in a total gravitational potential

$$\phi = \phi_{\star} + \phi_D, \quad (19)$$

where ϕ_{\star} is estimated from the N -particle model for the light distribution via a spherical harmonic decomposition (Sellwood 2003, DL07) assuming a constant mass-to-light ratio Υ , and ϕ_D is a dark matter halo potential with the logarithmic parametrization

$$\phi_D(R, z) = \frac{v_0^2}{2} \ln(r_0^2 + R^2 + \frac{z^2}{q^2}). \quad (20)$$

Moreover, the mass-to-light ratio is not a fixed parameter, but rather it is determined simultaneously with the modelling of the dynamical structure in the NMAGIC run.

For both galaxies, the slit data show clear rotation along the major axis on the sky. However, the regularization scheme as developed in Section 2.3.1 for spherical systems discourages any rotation in the particle model, as it biases individual weights towards the same prior regardless of the sense of rotation of the particles. Thus, in the following tests we adopt a modified setup for the grid of priors, binning particles according to E and x , and also according to the sign of their L_z , and assigning individual priors that differ between particles with different sense of rotation. For an axisymmetric potential, this effectively uses the total angular momentum L as an approximate third integral, which may be expected to be a reasonable first approximation unless $L \simeq L_z \simeq 0$ (Gerhard & Saha 1991).

6.1 The case of NGC 4697 and its halo

The intermediate luminosity elliptical galaxy NGC 4697 is seen almost edge-on. Assuming that the observed nuclear dust-lane is settled in the equatorial plane, Dejonghe et al. (1996) derived an inclination $i = 78^\circ \pm 5^\circ$, which is consistent with the bulge-disk decomposition of Scorza et al. (1998) if the disk component has an intrinsic axis ratio $h/R \sim 0.2$.

NGC 4697 has fitted Sersic model index $n = 3.5$, and an effective radius $R_{\text{eff}} \approx 66'' = 3.36$ kpc at an assumed distance $D = 10.5$ Mpc. Kinematic data show significant major axis rotation reaching ~ 100 km/s at $90''$.

NMAGIC axisymmetric particle models assuming an inclination $i = 80^\circ$ were constructed for NGC 4697 (DL08) fitting simultaneously surface brightness photometry, long-slit

absorption-line kinematics and hundreds of PNe velocities. A range of quasi-isothermal halos was found to be consistent with the observational constraints, and a massive halo with circular velocity $v_0 = 250$ km/s at $4.3R_{\text{eff}}$, referred to as model J in the notation of DL08, fits the PN data best. This model is characterized by a moderately radially anisotropic orbit distribution, with the anisotropy parameter $\beta \sim 0.3$ at the center and increasingly higher in the outer regions.

These models were constructed using the traditional GWR, and the μ parameter was set to 100 to avoid strong biases to the initial conditions. This in turn led to some overfitting of the slit kinematics data, especially for the higher order kinematic moments (see DL08 for details).

Thus we now build a new regularized J model of NGC 4697, to see whether a similarly good but smoother particle model can be obtained with the help of the new MPR. We rerun that exact model with the code NMAGIC using the new regularization scheme, and $\mu = 10^5$, and using constraints from both photometric and kinematic data, including PNe. As specified above, we bin particles according to their integrals E , x , and L_z when adopting the new regularization method, to allow for the rotation seen in the slit data.

A comparison of the final particle models obtained by DL08 and with this new MPR is shown in Figs. 12 and 13. Fig. 12 shows the projected absorption line kinematics of the final particle models overplotted on the data points. As discussed in DL08, asymmetries between the left-hand side and right-hand side in the profiles do not imply deviations from axisymmetry or equilibrium, but rather they are due to averages over slightly different slit cells on both sides. As expected, these asymmetries decrease when using the new MPR, which allows a higher amount of regularization, and the model profiles are indeed smoother than for the DL08 model.

The intrinsic kinematics of the final particle models are compared in Fig 13: the velocity anisotropy increases from the center outwards when adopting either GWR or MPR, but MPR results in much smoother profiles in the regions constrained by data.

6.2 The case of NGC 3379 and its halo

In DL09 a sequence of spherical and axisymmetric NMAGIC models fitting an extensive data set (photometry, long-slit and SAURON absorption-line kinematics, PN velocity dispersion data) was constructed to investigate the mass distribution and orbital structure of the intermediate luminosity E1 galaxy NGC 3379.

No independent information on the inclination is available for this galaxy, and values of $i > 40^\circ$ are consistent with the photometry. The effective radius $R_{\text{eff}} \approx 47'' = 2.23$ kpc at an assumed distance $D = 9.8$ Mpc. The combined kinematic data set shows major axis rotation reaching ~ 50 km/s at $20''$, with PNe indicating a further increase to ~ 70 km/s at $220''$.

DL09 explored a sequence of spherical and axisymmetric models, together with some triaxial test models. They found that their results were insensitive to the adopted geometry. Both strongly radially anisotropic models embedded in massive dark matter halos and nearly isotropic systems dominated by the stellar mass are consistent with the

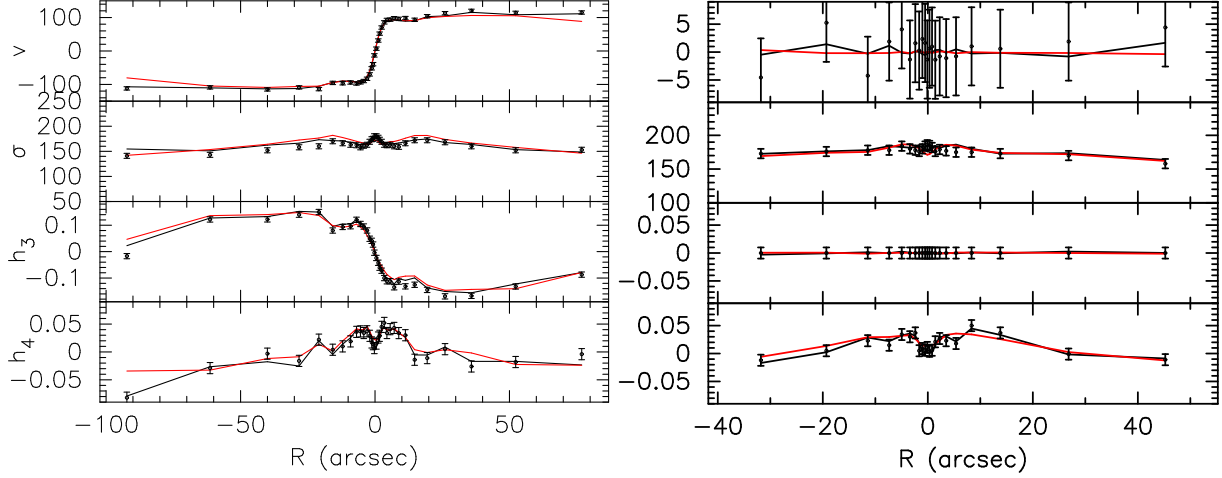


Figure 12. Particle model fits to the slit data of NGC 4697 along the major (*left*) and minor axis (*right*). The model data points are averages over the same slit cells as the target data, and are connected by straight line segments. The *black line* shows model J of DL08, while the *red line* shows the same model obtained using the new MPR.

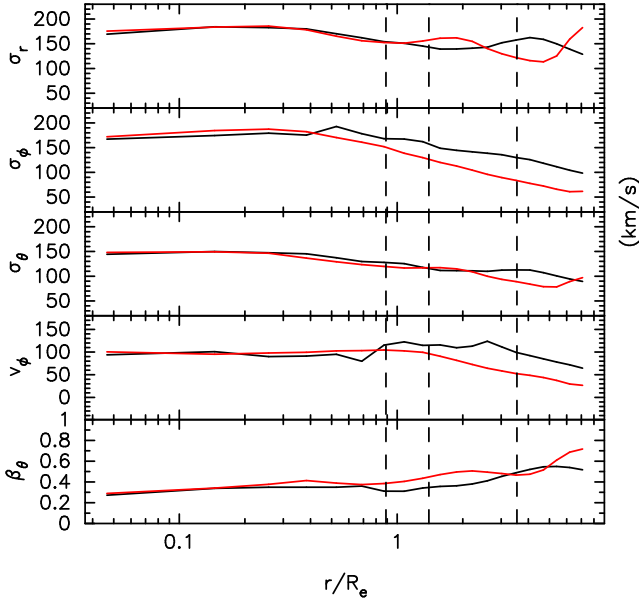


Figure 13. Internal velocity moments in the equatorial plane for model J of DL08 (*black line*) and the new regularized J model obtained here (*red line*), for NGC 4697. The vertical dashed lines indicate the radial extent of the minor axis slit data, major axis slit data, and PN data, from left to right.

data. I.e., even the extensive data set used in the modelling was not sufficient to break the mass-anisotropy degeneracy (Binney & Mamon 1982) because of the rapidly decreasing velocity dispersion profile for NGC 3379. However, an analysis of the quality of the fit and of the likelihood of the observed PN velocity data for the spherical models slightly favoured a range of models centered around the radially anisotropic halo C, which was obtained for a quasi-isothermal potential in equation (20), with $r_0/R_{\text{eff}} = 3$, $v_0 = 130$ km/s, and $q = 1$.

We now reconstruct that spherical C model with the new MPR method. Given the data setup is very similar to the one adopted in the tests of Section 5, we set $\mu = 10^6$. We

bin particles according to their integrals E , x , and L_z , because of the observed rotation in both the slit and SAURON data. For the energy grid we use a linear binning of the function $\exp(E)$, which provides a better sampling of the model DF in the outer regions for this potential.

Fig. 14 shows the fit to SAURON data for the final NMAGIC models obtained with GWR and MPR. Both particle models reproduce the observed rotation with great accuracy, and the MPR model is clearly smoother than the original (symmetrized) data. In particular, notice the ring-like structure in the h_4 plot. Even though the new model is generated using a much higher value of μ , i.e. much stronger smoothing, it still does a good job in fitting the observational data, with $(\chi^2/J)_{\text{sauron}} = 0.86$ (compared to 0.17 for the traditional GWR).

The intrinsic kinematics of the final NMAGIC models (Fig. 15) are similar, but using MPR the kinks in the profiles disappear. It can be seen that a strong radial anisotropy is required to match the PNe data in this dark matter halo.

7 DISCUSSION AND CONCLUSIONS

Building on the work of ST96, successive investigations (DL07; DL08; DL09; Dehnen 2009; Long & Mao 2010) have shown the power of the χ^2 M2M modelling technique to learn about the dynamics of galaxies. χ^2 M2M methods work by adapting the weights of an N -body particle system until the observational data are well matched in a χ^2 sense, subject to additional regularization constraints. These constraints are needed to prevent the particle model from acquiring large fluctuations because of scatter and noise especially in the kinematic data.

Traditionally, a Global Weight entropy Regularization (GWR) is adopted to regularize the underlying particle system. However, through constant flat priors GWR introduces a bias in the particle model which makes it difficult to reproduce strong phase-space gradients of the target galaxy, e.g. anisotropic velocity distributions, unless its dynamical structure is known beforehand.

In this paper we have described a new Moving Prior

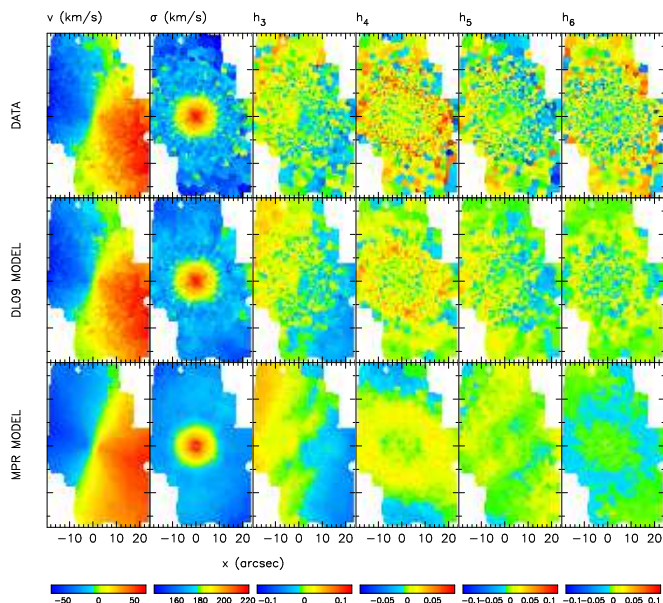


Figure 14. Particle model fits to the SAURON integral field kinematic data for NGC 3379. Top row: symmetrized SAURON data. Middle row: best-fitting C model (DL09). Bottom row: new regularized C model. Mean velocity, velocity dispersion, and higher order Gauss-Hermite moments are shown in the panels from left to right.

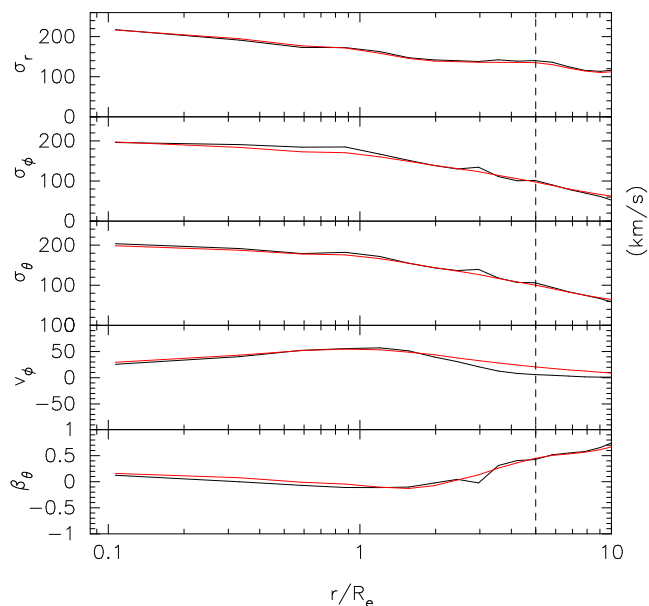


Figure 15. Internal velocity moments in the equatorial plane for model C of DL09 (black) and the new regularized C model obtained here (red), for NGC 3379. The vertical dashed line marks the last data point.

Regularization (MPR) method, based on a prior distribution for the particles which evolves with the model. Individual particle priors are updated along with particle weights to keep track of the phase-space structures of the evolving weight distribution. The basic idea is to determine the priors such that they are similar for particles on neighbouring orbits, specified by orbital invariants or integrals of motion such as energy and angular momentum in the spherical case.

The new priors are then used in a weight entropy function to ensure a regularization which smoothes locally in phase-space, without erasing global phase-space gradients.

We have then tested this MPR scheme, together with the χ^2 M2M modelling technique, using a series of spherical target galaxies with both idealized and realistic data. Our main conclusions are as follows:

- For a truncated spherical target galaxy with idealized data, for which in theory a unique inversion of the data exists, our NMAGIC models with MPR show that the target can be recovered accurately, and independent of the initial particle model.
- The new MPR generally improves both the accuracy with which the dynamical structure of the target galaxy is reproduced, and the convergence to the true solution independent of the initial particle model. Compared to GWR, biases in the anisotropy structure are removed, and local fluctuations in the intrinsic distribution function are reduced. Moreover, MPR allows a higher amount of smoothing than the weight entropy regularization, while the data are still fitted well.
- Lack or poorer quality of data introduce degeneracies in the dynamical modelling results and a dependence on the initial particle model, so that the reliability of the models is limited to those regions in which good observational data exist. Also in this case, the new MPR achieves a better reconstruction of the target properties and is less dependent on the choice of the initial particle model.
- Using the new MPR, we have reconstructed the best-fitting NMAGIC models determined in previous work by DL08 and DL09 for the two elliptical galaxies NGC 4697 and NGC 3379 in their dark matter halos. To this goal, we have extended the MPR method to the axisymmetric case, using the integrals E and L_z and the total angular momentum as an approximation to the third integral. The final models are intrinsically smoother and provide smoother fits to the available data.

There is clearly room for improving the current version of MPR: the method could be generalized to systems of lower symmetry using the invariants associated with orbits, *e.g.* the turning points, to assign moving priors in phase-space to the particles. Moreover, a cumulative grid-less variant of the method could also be implemented. Re-sampling of the N -body system from time to time during and after the adjustment of the weights (Dehnen 2009) would enforce equal weight for particles orbiting the same torus, but it would not take care of smoothing between nearby tori with very different weights.

To conclude, the experiments described in this paper show that the moving prior regularization method improves the correct and unbiased recovery of the orbit structure of the target galaxy from noisy data. A similar regularization scheme could also be implemented in Schwarzschild orbit superposition models.

ACKNOWLEDGMENTS

We thank Karl Gebhardt for making his smoothing spline code available, and an anonymous referee for a careful read-

ing of the paper. LM acknowledges support from and participation in the International Max-Planck Research School on Astrophysics at the Ludwig-Maximilians University.

REFERENCES

- Binney J., 2010, *MNRAS*, 401, 2318
- Binney J., Mamon G. A., 1982, *MNRAS*, 200, 361
- Binney J., Tremaine S., 2008, *Galactic Dynamics: Second Edition*. Princeton University Press
- Binney J. J., Davies R. L., Illingworth G. D., 1990, *ApJ*, 361, 78
- Bissantz N., Debattista V. P., Gerhard O., 2004, *ApJ*, 601, L155
- Cappellari M., 2008, *MNRAS*, 390, 71
- Cappellari M., Bacon R., Bureau M., Damen M. C., Davies R. L., de Zeeuw P. T., Emsellem E., Falcón-Barroso J., Krajnović D., Kuntschner H., McDermid R. M., Peletier R. F., Sarzi M., van den Bosch R. C. E., van de Ven G., 2006, *MNRAS*, 366, 1126
- Cappellari M., di Serego Alighieri S., Cimatti A., Daddi E., Renzini A., Kurk J. D., Cassata P., Dickinson M., Franceschini A., Mignoli M., Pozzetti L., Rodighiero G., Rosati P., Zamorani G., 2009, *ApJ*, 704, L34
- Cappellari M., Verolme E. K., van der Marel R. P., Kleijn G. A. V., Illingworth G. D., Franx M., Carollo C. M., de Zeeuw P. T., 2002, *ApJ*, 578, 787
- Carollo C. M., de Zeeuw P. T., van der Marel R. P., 1995, *MNRAS*, 276, 1131
- Cretton N., de Zeeuw P. T., van der Marel R. P., Rix H., 1999, *ApJS*, 124, 383
- Das P., Gerhard O., Churazov E., Zhuravleva I., 2010, *MNRAS*, 409, 1362
- Das P., Gerhard O., Mendez R. H., Teodorescu A. M., de Lorenzi F., 2011, *MNRAS*, 415, 1244
- de Lorenzi F., Debattista V. P., Gerhard O., Sambhus N., 2007, *MNRAS*, 376, 71
- de Lorenzi F., Gerhard O., Coccato L., Arnaboldi M., Cappacchioli M., Douglas N. G., Freeman K. C., Kuijken K., Merrifield M. R., Napolitano N. R., Noordermeer E., Romanowsky A. J., Debattista V. P., 2009, *MNRAS*, 395, 76
- de Lorenzi F., Gerhard O., Saglia R. P., Sambhus N., Debattista V. P., Pannella M., Méndez R. H., 2008, *MNRAS*, 385, 1729
- Debattista V. P., Sellwood J. A., 2000, *ApJ*, 543, 704
- Dehnen W., 2009, *MNRAS*, 395, 1079
- Dehnen W., Gerhard O. E., 1993, *MNRAS*, 261, 311
- Dehnen W., Gerhard O. E., 1994, *MNRAS*, 268, 1019
- Dejonghe H., 1986, *Physics Reports*, 133, 217
- Dejonghe H., de Bruyne V., Vauterin P., Zeilinger W. W., 1996, *A&A*, 306, 363
- Dejonghe H., de Zeeuw T., 1988, *ApJ*, 333, 90
- Dejonghe H., Merritt D., 1992, *ApJ*, 391, 531
- Gebhardt K., Richstone D., Tremaine S., Lauer T. R., Bender R., Bower G., Dressler A., Faber S. M., Filippenko A. V., Green R., Grillmair C., Ho L. C., Kormendy J., Magorrian J., Pinkney J., 2003, *ApJ*, 583, 92
- Gerhard O., Jeske G., Saglia R. P., Bender R., 1998, *MNRAS*, 295, 197
- Gerhard O. E., 1991, *MNRAS*, 250, 812
- Gerhard O. E., 1993, *MNRAS*, 265, 213
- Gerhard O. E., Saha P., 1991, *MNRAS*, 251, 449
- Hernquist L., 1990, *ApJ*, 356, 359
- Hernquist L., Ostriker J. P., 1992, *ApJ*, 386, 375
- Hunter C., de Zeeuw P. T., 1992, *ApJ*, 389, 79
- Hunter C., Qian E., 1993, *MNRAS*, 262, 401
- Kronawitter A., Saglia R. P., Gerhard O., Bender R., 2000, *A&AS*, 144, 53
- Kuijken K., 1995, *ApJ*, 446, 194
- Lokas E. L., 2002, *MNRAS*, 333, 697
- Long R. J., Mao S., 2010, *MNRAS*, 405, 301
- Magorrian J., 1995, *MNRAS*, 277, 1185
- Magorrian J., Binney J., 1994, *MNRAS*, 271, 949
- Matthias M., Gerhard O., 1999, *MNRAS*, 310, 879
- Merritt D., 1985, *AJ*, 90, 1027
- Merritt D., 1993, *ApJ*, 413, 79
- Merritt D., 1996, *AJ*, 112, 1085
- Osipkov L. P., 1979, *Pis ma Astronomicheskii Zhurnal*, 5, 77
- Press W. H., Teukolsky S. A., Vetterling W. T., Flannery B. P., 1992, *Numerical recipes in FORTRAN. The art of scientific computing*
- Richstone D. O., Tremaine S., 1985, *ApJ*, 296, 370
- Richstone D. O., Tremaine S., 1988, *ApJ*, 327, 82
- Rix H., de Zeeuw P. T., Cretton N., van der Marel R. P., Carollo C. M., 1997, *ApJ*, 488, 702
- Rodionov S. A., Athanassoula E., Sotnikova N. Y., 2009, *MNRAS*, 392, 904
- Schwarzschild M., 1979, *ApJ*, 232, 236
- Schwarzschild M., 1993, *ApJ*, 409, 563
- Scorza C., Bender R., Winkelmann C., Capacchioli M., Macchetto D. F., 1998, *A&AS*, 131, 265
- Sellwood J. A., 2003, *ApJ*, 587, 638
- Syer D., Tremaine S., 1996, *MNRAS*, 282, 223
- Thomas J., Jesseit R., Saglia R. P., Bender R., Burkert A., Corsini E. M., Gebhardt K., Magorrian J., Naab T., Thomas D., Wegner G., 2009, *MNRAS*, 393, 641
- Thomas J., Saglia R. P., Bender R., Thomas D., Gebhardt K., Magorrian J., Corsini E. M., Wegner G., 2005, *MNRAS*, 360, 1355
- Thomas J., Saglia R. P., Bender R., Thomas D., Gebhardt K., Magorrian J., Corsini E. M., Wegner G., 2007, *MNRAS*, 382, 657
- Thomas J., Saglia R. P., Bender R., Thomas D., Gebhardt K., Magorrian J., Richstone D., 2004, *MNRAS*, 353, 391
- Valluri M., Merritt D., Emsellem E., 2004, *ApJ*, 602, 66
- van den Bosch R. C. E., de Zeeuw P. T., 2010, *MNRAS*, 401, 1770
- van der Marel R. P., Cretton N., de Zeeuw P. T., Rix H., 1998, *ApJ*, 493, 613
- van der Marel R. P., Franx M., 1993, *ApJ*, 407, 525
- Wahba G., ed. 1990, *Spline models for observational data*
- Williams M. J., Bureau M., Cappellari M., 2009, *MNRAS*, 400, 1665
- Young P., 1980, *ApJ*, 242, 1232